
Proceedings Paper:
Bello, S. orcid.org/0000-0002-2065-4779, Urwick, A., Bastianini, F. et al. (2 more authors) (2022) An introduction to perovskites for solar cells and their characterisation. In: McNeilly, T., (ed.) Energy Reports. Multi-CDT Conference on Clean Energy and Sustainable Infrastructure, 05-06 Apr 2022, Sheffield, UK. Elsevier BV , pp. 89-106.

https://doi.org/10.1016/j.egyr.2022.08.205

Available online at www.sciencedirect.com
ScienceDirect
Energy Reports 8 (2022) 89–106
www.elsevier.com/locate/egyr

Multi-CDT Conference on Clean Energy and Sustainable Infrastructure, Professor Solomon Brown, 5th and 6th April 2022, the University of Sheffield

An introduction to perovskites for solar cells and their characterisation

Suleiman Bello*, Adam Urwick, Francesco Bastianini, Alisyn J. Nedoma, Alan Dunbar

Department of Chemical and Biological Engineering, University of Sheffield, United Kingdom

Received 11 August 2022; accepted 14 August 2022
Available online 27 August 2022

Abstract

Perovskite solar cells are one of the most active areas of renewable energy research at present. The primary research objectives are to improve their optoelectronic properties and long-term stability in different environments. In this paper, we discuss the working principles of hybrid perovskite photovoltaics and compare them to the competing photovoltaic technologies of inorganic and organic photovoltaics. The current challenges that hinder the commercialisation of perovskite solar cells are then discussed. This is followed by a description of perovskite material properties and some characterisation techniques commonly used to assess perovskite properties, fabrication processes including the use of antisolvents, and degradation mechanisms. We intend that this work should serve as a beginner's guide to the study of perovskite solar cells.

Peer-review under responsibility of the scientific committee of the Multi-CDT Conference on Clean Energy and Sustainable Infrastructure, Professor Solomon Brown, 2022.

Keywords: Characterisation; Crystallography; Devices; Excitonic; Efficiency; Materials; Optoelectronic; Perovskite; Tunability

1. Introduction

The importance of sustainable electric power generation cannot be overemphasised, as it is instrumental to every nation's economy and societal wellbeing. Fossil fuels have been the conventional source of electric energy over the last few centuries; however, the negative emissions from these energy sources have motivated researchers to seek alternative means of generating power that is sustainable in terms of the environment and human health. This has resulted in the widespread growth of renewable energy technologies such as hydroelectric, wind, solar (thermal and photovoltaic), tidal, and wave power. Most of these technologies derive their energy from the sun either directly or indirectly. On a clear day, the earth receives 173,000 TW/h of energy from the Sun [1]. While the world energy consumption before the Covid-19 lockdown was around 170,000TWh [1]. Therefore, direct conversion of solar energy into electricity using photovoltaics is an abundant alternative source to replace fossil fuels for electric power generation. The discovery of quantum theory and the photovoltaic effect in the early 20th century led to breakthroughs that enabled the development of solar cell technologies [2]. Photovoltaic (PV) devices are made

* Corresponding author.
E-mail address: sabello1@sheffield.ac.uk (S. Bello).

https://doi.org/10.1016/j.egyr.2022.08.205

Peer-review under responsibility of the scientific committee of the Multi-CDT Conference on Clean Energy and Sustainable Infrastructure, Professor Solomon Brown, 2022.

of semiconductors that absorb solar irradiation (light) to excite electrons, resulting in electron–hole pairs that are further separated and transported to the devices' contacts and from where the electrons and holes flow through the external circuit to generate electric current. This phenomenon is referred to as the photovoltaic effect [3]. Because of its potential as a clean and widely available source of electricity, the photovoltaic effect has been studied extensively in recent decades using different combinations of inorganic semiconductors, thin-film semiconductors, organic, and hybrid organic–inorganic materials. These can be categorised according to the physical principles by which they operate, that is they are either a p–n junction device; an excitonic device; or a p–i–n device. Conventional photovoltaics are typically made from Si and 25.1% power conversion efficiency was reported for thin-film Si-crystals [4].

Perovskite solar cells (PSCs) derived their name from the light-harvesting layer within the device which is made of perovskite-structured compounds. Typically, these are hybrid organic–inorganic halide-based materials such as methylammonium lead-halide ($CH_3NH_3PbX_3$), or a complete inorganic-halide material e.g., caesium lead-halide ($CsPbX_3$) perovskite film. Perovskites were first proposed as a visible light sensitiser for PVs in 2009 with a laboratory-scale device efficiency of 3.8% achieved [5]. However, since then single-junction perovskite solar cells (PSCs) have reached laboratory power conversion efficiencies (PCEs) of 25.5%, while for tandem perovskite/silicon PVs, PCEs >29% have been reported [6].

2. n–i–p/ p–i–n PV devices

Planar perovskite solar cells (PSCs) can be made in either a regular n–i–p structure or an inverted p–i–n structure (see Fig. 1 for the meaning of n–i–p and p–i–n as regular and inverted architecture), They are made from either organic–inorganic hybrid semiconducting materials or a complete inorganic material typically made of triple cation semiconductors that absorb the incident solar radiation [7]. The conventional single-junction architecture of these devices is similar to the architecture used in bilayer heterojunction organic photovoltaics. However, the physical mechanism by which perovskite PVs operates is different to that of organic PVs. The exciton binding energy in perovskite materials is much lower than in OPV materials so excitons are not formed at room temperature. Therefore these devices require the effective application of an electron transporting layer (ETL) or p-type layer and a hole transporting layer (HTL) n-type layer to assist with separation of the mobile and unbound charge carriers according to their charge [8]. In some planar perovskite PVs, a mesoporous buffer layer is added after depositing the ETL to boost the PCE of the PSC by reducing the Jsc-Voc hysteresis [9].

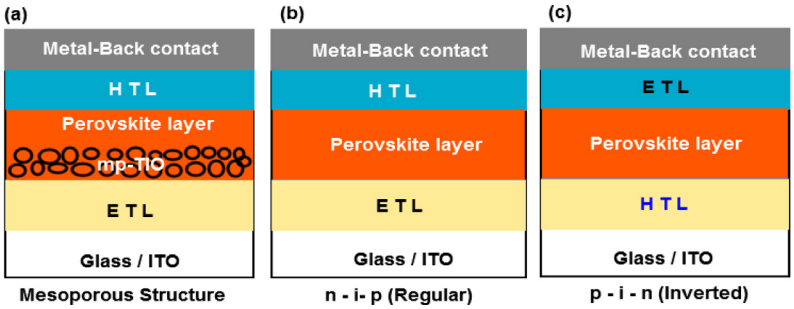

Fig. 1. The three schematic illustrations of perovskite PV device architecture.

The mechanism by which perovskite photovoltaics operates is that the absorbing layer is made of perovskite materials that generate energetically excited free mobile charge carriers upon illumination. [9]. This is because the excitonic binding energy in perovskite is comparable to the thermal energy readily available and therefore excitons are either not generated or immediately dissociated resulting in free electrons and holes which can act as charge carriers. These carriers have high mobility and can travel to the conduction band (LUMO) of the ETL and or the valence band (HOMO) of the HTL, Fig. 2a [9]. From the ETL and HTL, the electrons and holes respectively are transported through to the cathode/anode to generate an electric current in an external circuit as shown in Fig. 2b. One challenge with PSCs is instability materials that make up the perovskite, ETL and HTL layers because they are sensitive to changes in environmental conditions. A second challenge is the toxicity of the typically lead-based perovskites used, due to the possibility of lead leakage when the cells degrade over time [10].

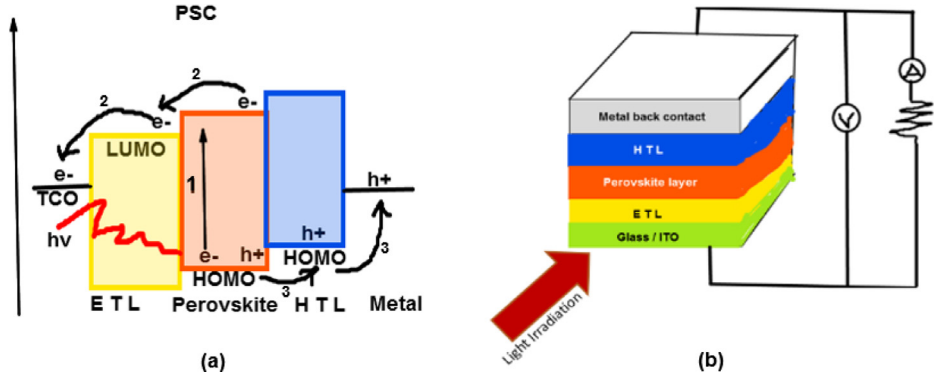

Fig. 2. (a) Schematic working principle of PSC and (b) Circuit connection of the perovskite solar cell.

The efficiency of PSCs can be further increased by forming tandem or multi-junction solar cells. These consist of two to more absorbing layers with different energy gaps (to absorb different parts of the solar spectrum) within a single device. However, this literature review focuses on single-junction perovskite solar cells to introduce the attractive properties of perovskites and the challenges they must overcome before global commercialisation of PSCs can become a reality.

2.1. p–n junction PV devices

The current market leading solar cell technologies are p–n junction PV devices. These are typically made from inorganic materials such as silicon, germanium, gallium arsenide, and copper indium gallium sulphide or cadmium telluride. Whilst silicon is the most widely used material it is an indirect semiconductor and therefore has poor absorbance. The first-generation solar cell devices made from Si therefore needed typically relatively thick layers of monocrystalline silicon. When thin films of alternative direct band gap semiconducting materials were used they were referred to as second-generation solar cells [11].

The basic working principle of these PV cells relies upon the electronic structure created at the junction between two regions of a semiconductor that have been doped with two different elements, to create so-called p-type and n-type doping. The most common example is silicon doped with boron and phosphorous to create p-type and n-type Si respectively. n-type doping incorporates atoms with more electrons than the intrinsic semiconductor into the crystal lattice and this results in extra electrons available for charge transport being available within the n-type semiconductor. Conversely, p-type doping incorporates atoms with fewer electrons within the crystal lattice resulting in electron vacancies or holes within the crystal which behave as positive charge carriers (both n-type and p-type semiconductors remain charge-neutral overall due to the additional proton in the n-type dopant atoms and the reduced number of protons in the p-type dopant atoms). At the p–n junction between a region of p-type doped semiconductor and another region of n-type doped semiconductor the uneven distribution of electrons and holes on either side of the junction attempts to reach equilibrium by the diffusion of electrons from the n-type material into the p-type material, and the diffusion of holes from the p-type into the n-type. The net effect of this diffusion is the creation of a region where the surplus charge carriers introduced by doping are depleted. The electrons diffuse across the junction into the p-type material to fill the surplus holes and similarly holes diffuse across the junction to combine with the surplus electrons in the n-type material near the junction. This region is therefore referred to as the depletion region. This diffusion of charge carriers results in the establishment of an electric field due to the spatial separation of charge, and the field acts so as to limit the extent of the diffusion. It does so by inducing a drift current that acts to oppose the diffusion and thereby limits the width of the depletion region. The diffusion of electrons and holes and the depletion region formed at the p–n junction within a PV device are represented in Fig. 3.

When a photon with sufficient energy (i.e., greater than the energy gap of the semiconductor the solar cell is made from) is absorbed, it excites an electron across the gap, leaving a holes in lower energy state. The electron will then rapidly relax down to the edge of the conduction band, and the hole relaxes upwards to the valence band

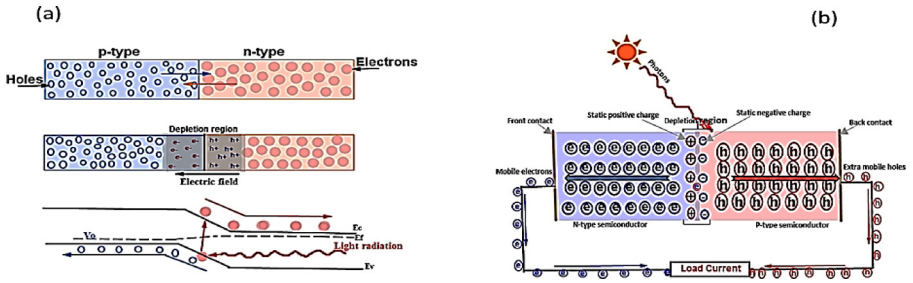

Fig. 3. (a) Schematic illustration of p–n PV device with energy levels, (b) The electrons and hole flow in a p–n PV circuit device.

edge losing energy as heat as they do so. This creates an extra electron and hole at the band edges which are mobile and free to transport their charge as shown in Fig. 3(a). If these photo generated charge carriers are created in the depletion region, the presence of the built-in electric field causes them to move creating a flowing current. The electrons flow within the conduction band towards the n-type side of the junction and the holes flow within the valence band towards the p-type side of the junction. This separation of photo-generated electrons and holes results in a potential difference/voltage build-up across the p–n junction. If suitable conducting electrodes are attached to either side of the junction, then this voltage can drive the photo-generated current through an external circuit as shown in Fig. 3(b).

Silicon-based PVs are presently the dominant type of solar cell in the global market. This is largely due to solar cell development benefitting from piggybacking on the technological development of Si as a material for the electronics industry, its natural abundance in the form of silicon oxide and its environmentally friendly chemical properties. However, Si as a photovoltaic material has some disadvantages, one of which is the indirect alignment between the valence maximum and conduction band minimum in crystalline Si. This indirect bandgap means a phonon is required in the photon absorption process to ensure momentum is conserved. This results in Si being a relatively poor absorber of light because it has a relatively weak extinction coefficient. To overcome this challenge, thick layers of crystalline silicon (c-Si) are needed to absorb sufficient solar energy for conversion into electricity. Consequently, a relatively large amount of Si is needed to make an efficient Si solar cell [12]. This increases the material processing costs and the thick Si layer needed will be inflexible. Moreover, thicker solar cells tend to suffer from power conversion efficiency losses due to electron traps or the occurrence of non-radiative recombination pathways for the charge carriers leading to lower power output [12,13]. This can be offset to some extent by using very high purity defect-free Si. However, producing high purity material increases the material production costs.

To overcome the negative impact of using thick layers of c-Si PVs, scientists have explored thin films of different semiconductors as the absorbing material for solar cells. These require smaller volumes of photoactive material, hence reducing the amount of material needed. Thin films of modified c-Si have also been used in solar cells which can absorb incident solar energy as effectively as a direct bandgap semiconductor. The Si is modified by doping with impurities such as boron, phosphorus or sulphur with surface passivation and interdigitated back contacts resulting in a significant improvement in its power conversion efficiency. Many direct bandgap semiconducting materials such as CdTe, CdS, and CIGS were found to have better laboratory solar energy conversions when used in thin-film solar cells. However, the lower global abundance of tellurium, cadmium toxicity and degradation under solar illumination have been challenging issues for such devices and further research is needed [13]. Gallium Arsenide (GaAs) thin film, single-junction solar cells have a direct bandgap close to the optimal and as such have exceptional electronic properties that make them stand out amongst the 2nd generation thin-film PVs. A PCE of 29.1% has been achieved for thin-film GaAs PV as reported by National Renewable Energy Laboratory [4] and this makes it a promising candidate to compete with Si PVs, however, at present they are prohibitively expensive and are mostly used for high values applications such as powering spacecraft and satellites [14].

2.2. Excitonic PV devices

Excitonic solar cells aim to compete with conventional, typically Si-based, solar cells and the most commonly studied excitonic PV devices are either organic photovoltaics (OPVs) or dye-sensitised solar cells (DSSCs).

Together these two categories are considered the third generation of solar cells technology. Compared to inorganic semiconductors such as c-Si, OPVs materials have much higher absorption coefficients and lower densities, such that a very thin film of active organic polymers and fullerene derivatives is sufficient to generate electric power when illuminated with incident light radiation of appropriate wavelength. Thus, this allows the use of less material during fabrication. Motivation to develop OPVs arises from their low fabrication cost, flexibility, lightweight, and tunability of the organic materials allowing optimisation of the material properties. However, the present record PCE of this class of solar cells is ∼18.2% [4], below that of c-Si. This is due to their low electron mobility's, energy loss during exciton dissociation and low dielectric constant. [15].

In comparison, the working principle of this solar cell is quite different from perovskite solar cells and inorganic p–n junction solar cells. When OPVs are illuminated, a localised and strongly bound exciton (i.e. a bound electron–hole pair) is generated, with the electron in the LUMO (lowest unoccupied molecular orbital) and the hole in the HOMO (highest occupied molecular orbital) energy level. Such strongly bound excitons are known as the Frenkel excitons, and they must be separated to enable the charge carriers to flow in opposite directions. This separation is best done as quickly as possible to minimise exciton recombination. Typically, it is achieved by introducing a donor–acceptor interface. In 1986, Tang invented a bilayer donor/acceptor heterojunction of OPVs which could separate the excitonic bond [16]. However, due to the short exciton diffusion length, the efficiency of bilayer OPVs is very limited as the exciton is likely to recombine before reaching the interface. To overcome this challenge, bulk heterojunction (BHJ) OPVs were fabricated where the donor and acceptor materials are mixed to form a bi-continuous network with a very small scale phase separation [17]. This allows most excitons to reach a donor–acceptor interface where they can then dissociate into electrons and holes within active layers. Fig. 4, compares the structures of the bilayer and bulk heterojunction devices commonly used to create the required donor–acceptor interfaces needed for exciton separation [8].

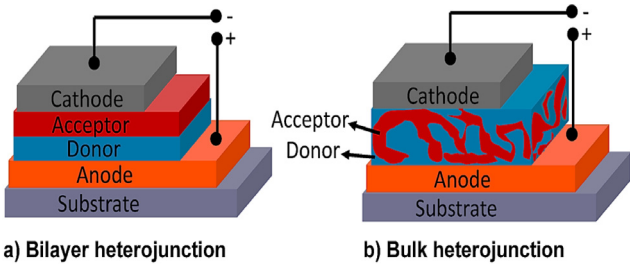

Fig. 4. Conventional architecture of the organic solar cell, with the donor materials shown in blue and acceptor materials in red [8].

After exciton generation by absorbing sunlight, the excitons diffuse to the donor–acceptor interface and dissociate with the electron and hole sacrificing enough of their energy to overcome the exciton binding energy. The electron subsequently falls into the acceptor material and the hole rises into the donor material at the interface between the electron acceptor and electron-donating semiconductors, as illustrated in Fig. 5 [18]. These charges are now free to travel to the appropriate electrode layers in the solar cell and therefore generate an electric current when connected to an external circuit and this could be seen in Fig. 4. The strong binding energy of the excitons generated in organic semiconductors means that the difference in the energy levels between the donor and acceptor materials must be sufficiently large to enable exciton dissociation. This results in some energy loss [19]. The most commonly used organic electron-donating species that function as hole-transporting materials are mostly conjugated polymers such as poly (3-Alkyl thiophenes), PEDOT: PSS, PCPDTBT, PTPT, PDPP3T, PSiF-DBT etc., whilst fullerene derivatives such as 6,6-phenyl-Carbonx-butyric acid methyl ester (PCxBM) have been widely used as electron acceptor and transporting materials. Due to fullerene crystallisation in an organic solvents which results in unfavourable phase separation, small molecules such as ITIC have been used as n-type materials in place of fullerene species [20,21]. Therefore, more recently these non-fullerene acceptors (NFAs) such as rylene-monoimides, rylene-diimides, tetracyano butadiene derivatives, pentacene derivatives etc. are now considered a more promising alternative to replace fullerene-based acceptors because of their tunability that enhances OPVs performance.

Dye-sensitised solar cells (DSSC) are also considered third-generation solar cells. They are made using a mesoporous nanocrystalline metal oxide (e.g., TiO_2) coated with a very thin layer of a sensitising dye

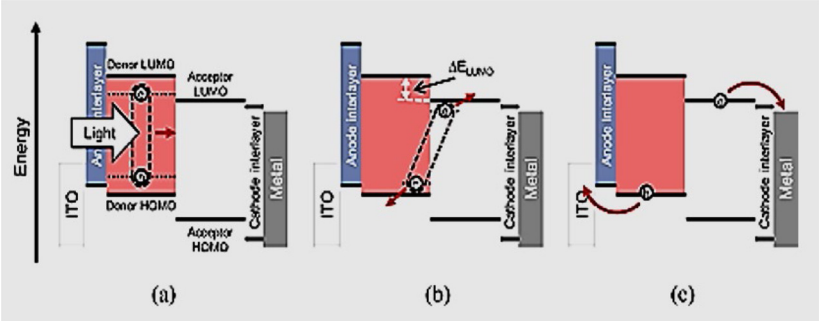

Fig. 5. Schematic illustration of OPV working principle [18].

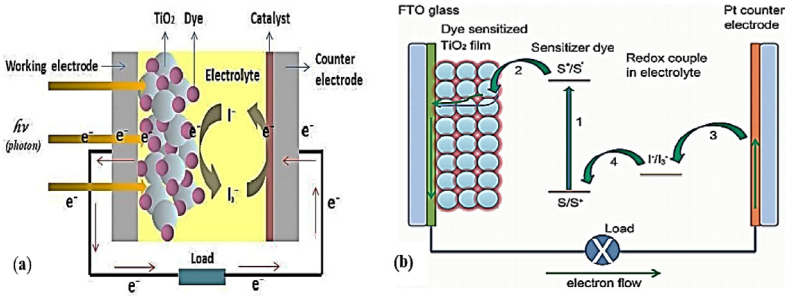

Fig. 6. (a) Conventional architecture of dye sensitises solar cell [22] (b) Schematic illustration of DSSCs working principle [23].

e.g., Ruthenium–polypyridine as the absorbing layer and the circuit is closed by a counter electrode (e.g., Pt) in a sandwich with a liquid iodide/triiodide electrolyte, as is shown in Fig. 6a [22]. An electric current is produced when the device is illuminated. The incident light enters the device and is absorbed by photosensitised dye material on the TiO_2, causing excitation of electrons from the conjugated dye bonds, excitons are generated and dissociate at the interface with the electrolyte. Electrons flow in direction of the anode, and holes in direction of the cathode. The oxidised sensitiser (i.e., S^+) accepts electrons (e^-) from the electrolyte (redox mediator). This regenerates the ground state of sensitiser (S) at expense of I^- ions, which are oxidised to elemental I which reacts with I^- to create I_3^-. I^- ions are generated in turn by the reduction of I_3^- ions at the platinum (Pt) counter electrode where electrons which have left the anode and travelled through the external circuit before they return to the cell from the external circuit via the Pt cathode. The complete circuit is presented in Fig. 6b [23]. DSSC are renowned for their flexibility and can be manufactured as semi-transparent cells. One of the major challenges of DSSCs is their efficiency. Also the cost and complex synthesis of the Ru-based dyes commonly used to sensitise the devices. Alternatives to the metal Ru complex such as natural dyes from organic plants are being considered [21]. Another challenge is the use of a liquid electrolyte as the charge carrier because the liquid may leak or freeze in unfavourable climates. All-solid-state DSSCs are being considered a promising approach to resolve this challenge [24,25].

3. Perovskite materials

Historically, the term perovskite refers to a naturally occurring mineral made of calcium titanium oxide ($CaTiO_3$) Fig. 7 [26], discovered in the Ural Mountains by scientists Gustav Rose in 1839. Rose named the mineral perovskite in honour of mineralogist Aleksevich Lev. Perovskite [27].

Today, an entire class of materials (both natural and synthetic) that adopt the same crystal structure are what we call perovskites. Their structures are all based on the same general chemical formula ABX_3. This crystal arrangement was described in 1926 by Victor Goldschmidt who also introduced a tolerance factor to determine the stability of perovskite materials [28]. Perovskites are now known to be the world's most abundant class of minerals and have long been of interest to geoscientists as they try to understand the formation of the Earth. Perovskites are researched widely in many different materials fields, from ferroelectrics, superconductors, and fuel

Fig. 7. Natural crystal image of perovskite mineral [26].

cells to spintronics, thermoelectrics and recently, photovoltaics. They owe this wide variety of applications to their renowned chemical tolerance and structural flexibility complemented by good physical and chemical properties. Their extensive adaptability and applicability form the basis of a $20-billion-dollar electro-ceramics industry in applications such as catalysts, insulators, semiconductors, superionic conductors and superconductors [29].

3.1. Perovskite crystal structure

The basic perovskite crystal ABX_3 has two positively charged cations (A & B), the A cation could be organic or inorganic materials while the B cations are mostly inorganic metals and one non-metallic negatively charged anion (X) mainly halogens or oxygen. The larger A-site cation sits at the centre of the tetragonal unit cell, while 8 B-site octahedron cations occupy the corners. The X-site anions fill the midpoints along the edge of the cell. If this is presented as an assembly of cubic polyhedrons, the cell can be interpreted as an A cation surrounded by 8 corner-sharing B cation-centred octahedrons, with X anions at the points of each octahedron, as shown in Fig. 8 [30].

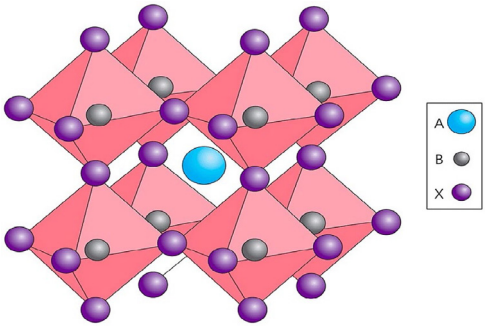

Fig. 8. Cubic crystal structure of perovskite [30].

Each site of the perovskite unit cell can be occupied by a vast array of different elements, with 24 elements identified as capable of occupying the A-site, 50 capable of occupying the B-site, while oxygen, SCN and halides can occupy the X-sites. This large range of possible combinations accounts for the incredible structural variety encapsulated within the broad perovskite family. If an A-site cation is too small relative to its B-site neighbours this can lead to a deviation from the ideal cubic structure resulting in tetragonal or orthorhombic structures, resulting in twisting, and tilting of its surrounding octahedrons to lower energy or even off-centring of cations resulting in polarity. Furthermore, the sites can also be occupied by a mix of cations i.e., more than one element can occupy the A-site, or differently charged ions of the same element, where the material can be consequently tuned along with a continuous series of compositional variance. In the field of perovskite solar cell research, the most studied materials are hybrid organic/inorganic metal halides. These complex compounds typically have A-site cations such as, methylammonium ($CH_3NH_3^+$), formamidinium ($CH(NH_2)_2\ ^+$) or caesium (Cs^+), with the B-site being occupied by a post-transition metal, such as lead (Pb^{2+}), tin (Sn^{2+}) or bismuth (with bismuth having more than one oxidation

state: -3, +1, +2, +3 or +5) [31] and X is a halogen anion such as bromine (Br^-), chlorine (Cl^-) or iodine (I^-) [30,31].

3.2. Perovskite tunability and optoelectronic properties

The hybrid organic–inorganic material $CH_3NH_3PbI_3$ ($MAPbI_3$) is one of the most studied perovskites, due to its excellent optoelectronic properties, e.g., low exciton binding energy (∼16 meV), direct–indirect bandgap energy of 1.51 to 1.55 eV, high electron and hole diffusion lengths (0.1 to 1 μm) and high electron and hole charge mobilities [32]. These make $MAPbI_3$ an efficient charge carrier and an excellent photoactive absorbing layer for solar cells with absorption coefficient ($\alpha = 81448\ cm^{-1}$), relative permittivity (dielectric constants $\epsilon_1 = 25.7$, or a high $\epsilon_2 = 5.6$) and extinction coefficient (k = 0.38085 cm^{-1}) [10]. However, due to its stability challenges in an ambient environment, different fabrication steps have been developed, such as mixing more than one cation and/or anions at different stoichiometries to fine-tune the bandgap energy of the perovskite which results in modification of the crystal structure from either orthorhombic or tetragonal to an asymmetrical cubic structure [33]. The cubic crystalline structure of perovskite was reported to be more stable under ambient conditions than orthorhombic and tetragonal perovskite structures [33]. Furthermore, the stability of the absorbing perovskite materials can be enhanced by carefully selecting a hydrophobic electron and hole transporting layer (ETL/ HTL) of a perovskite PV cell [34]. The introduction of a hydrophobic passivation layer and additives were also shown to improve the stability of perovskite devices [35]. A range of different cations and anions species have been used for the fabrication of thin-film perovskite solar cells over the past few decades as shown in Table 1 [36].

Table 1. The effective Ionic radii of A-cations, B-cations and X-anions for perovskite solar cells with the chemical formula ABX_3, [36].

A — Cations	rA (pm)	B — Cations	rA (pm)	X — Anions	rA (pm)
Ammonium $[NH_4]^+$	146	Bismuth $[Bi]^{3+}$	103	Bromine $[Br]^-$	196
Azetidinium $[(CH_2)_2NH_2]^+$	250	Cadmium $[Cd]^{2+}$	95		181
Caesium $[Cs]^+$	167	Copper $[Cu]^+$	77	Chlorine [Cl]	133
Ethylammonium $[CH_3CH_2NH_3]^+$	274	Copper $[Cu]^+$	73	$^-$	220
Formadinium $[CH(NH_2)_2]^+$	253	Germanium $[Ge]^{2+}$	73	Fluorine [F] $^-$	
Guanidinium $[(NH_2)_3C]^+$	278		120		
Hydrazinium $[NH_3NH_2]^+$	217	Lead $[Pb]^{2+}$	69	Iodine $[I]^-$	
Hydroxylammonium $[NH_3OH]^+$	216	Nickel $[Ni]^{2+}$	80		
Imidazoline $[C_3N_2H_5]^+$	258	Platinium $[Pt]^{2+}$	94		
Methylammonium $[CH_3NH_3]^+$	217	Silver $[Ag]^{2+}$	115		
Potassium $[K]^+$	138	Silver $[Ag]^+$	115		
Rubidium $[Rb]^+$	149	Tin $[Sn]^{2+}$	74		
3-pyrollinium $[NC_4H_8]^+$	272	Zinc $[Zn]^{2+}$			

3.3. Perovskite crystallographic stability

Perovskite crystal and structural stability can be determined based on a model established by V. M. Goldschmidt, which is a deviation of a spherical model which uses the effective ionic radius of the ions within the ABX_3 perovskite structure. T, where r_A, r_B, and r_X are the effective ionic radii of A, B and X ions, respectively.

$$\tau = \frac{(r_A + r_X)}{\left[\sqrt{2}\,(r_B + r_X)\right]} \tag{1}$$

The phase stability of the cubic perovskite phase increases, the closer τ is to 1. Lower τ values lead to lower symmetry orthorhombic or tetragonal phases, while larger values can lead to layered structures, where the 3D network deviates into 2D structures consisting of alternating planes of the inorganic metal-halide octahedra and monolayers or bilayers of organic cations. Mixing very large (A_L) and small (A_S) cations can result in quasi-2D structures, where variable thickness perovskite layers are terminated by large organic cations. These are commonly referred to as Ruddlesden–Popper phases when the A_L is monovalent or Dion-Jacobson when A_L is divalent [37]. For hybrid perovskites, stability of the perovskite phase is expected within the range $0.813 < \tau < 1.107$, while the highest tolerance factor limit for hybrid iodide perovskite is between 1.06 and 1.0 [38]. The pseudo-binary

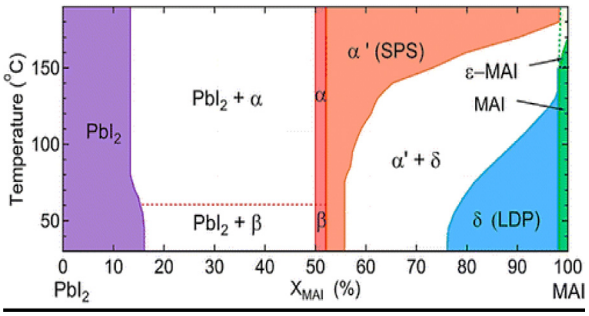

Fig. 9. Pseudo-binary phase diagram of MAPbI3 as a function of temperature [39].

phase diagram (see Fig. 9) [39], for the prototypical hybrid perovskite $MAPbI_3$ system, shows how altering the ratio of PbI_2 to MAI used during synthesis changes the perovskite phase as a function of temperature. $MAPbI_3$ has an I4/mcm tetragonal structure (β) at room temperature, where the c-axis is elongated due to the polar organic cation $CH_3NH_3^+$. Above 60 °C, relaxation of the structure as the degree of disorder decreases makes a secondary tetragonal phase (α) stable. This phase has often been conflated with a high temperature cubic phase due to the small elongation along the c-axis, which can be difficult to resolve [39].

Structural alterations will also arise from compositions that are non-stoichiometric, where there are vacancies of cations or anions in the structure, extra species squeezed into the crystal at interstitial sites, or antistitial defects [40]. Collectively these can be referred to as point defects. These defects can locally dope the perovskite, introduce trap states, and mediate hysteresis. These changes will affect their physical and optoelectronic properties such as conductivity and photoluminescence. Solution-processed hybrid perovskites have a high density of defects due to the imperfect crystallisation inherent in solution processing. Despite their high defect density perovskites remain remarkably efficient photovoltaics, and this is due to their high defect tolerance [41]. Point defects form transition level states either near the valence band maximum (VBM) or conduction band minimum (CBM), or states within the band gap of the perovskite. These are called trap states, and those which trap two types of carriers become recombination centres for free electrons and holes. Trap states near the band edges are called shallow-level traps, and de-trapping of carriers occurs more readily, as there is a lower energy offset. In perovskites, intrinsic defects such as vacancies most commonly form shallow level trap states. Deep trap states within the band gap form transition levels which in perovskites can be related to interstitial and anti-sites defects, also called Shockley–Read–Hall (SRH) recombination centres; they are responsible for trap-mediated non-radiative recombination and most typically arise at grain boundaries and surfaces [42]. Many approaches to improving the performance of hybrid perovskites as photovoltaics attempt to remove these trap states or counteract them, for example by improving crystallinity (film quality), passivation, and interfacial engineering [43]. Thus, increases in radiative efficiency are typically correlated with a reduction in deep-level trap states [44]. Along the same line, ion migration in PSCs has been a phenomenon that hinders the stability of the solar cell, and this is due to the ionic nature of perovskite materials and cannot be mitigated by simple encapsulation. The migrating ionic species could be intrinsic ions within perovskite crystal lattices such as MA^+, I^-, or extrinsic ions from interfacial layers e.g., Li^+, H^+, Na^+, etc. Eames et al. reported the activation energy of three ion migration mechanisms where I^- travels along the octahedral edge with low activation energy, MA^+ shifts to the neighbouring octahedral vacancy with moderate activation energy and Pb^{2+} moves with the highest activation energy [45]. It is commonly reported that in $MAPbI_3$ perovskite, I^- and MA^+ are the species that migrate most easily while Pb^{2+} seldom migrates much.

4. UV–Vis absorbance characterisation

UV–Vis absorbance analysis is a non-destructive method of characterisation that describes the optical absorption properties of a material. The fundamental mechanism by which perovskite materials absorb light is through intra-band light absorption [46]. However, light could also be absorbed by the semiconductor through inter-band, impurities, excitons, and the crystal lattice, which results in the determination of bandgap energy of the perovskite semiconductor [47]. The energy bandgap is the minimum quantum energy that is sufficient to excite an electron

from the highest valence energy level (Valence band) to the lowest conduction band energy level (Conduction band) and this leads to the formation of an absorption peak that indicates the excitation of electrons. In addition, a semiconductor with an indirect energy bandgap will require a high number of incident photons of light energy to cause excitation due to the release of a phonon during the light absorption process (this reduces the probability of absorbance occurring). The bandgap energy of a perovskite semiconductor with a direct valence–conduction band alignment could be determined using the quantum mechanics equation [48], given by:

$$E_g = \frac{hv}{\lambda} \tag{2}$$

The distribution of allowed electron transitions in a semiconductor with direct or indirect energy bandgap can be determined by applying the Tauc's model [48], and is described by the absorption coefficient (α), given as:

$$\alpha_{direct} = A\frac{(hv - Eg)^{\frac{1}{2}}}{hv} \tag{3}$$

$$\alpha_{indirect} = B\frac{(hv - Eg)^2}{hv} \tag{4}$$

Where, α = Absorption coefficient, A and B = UV–Vis absorption peak intensity, h = Plank's constant (6.626×10^{-34} Js), υ = speed of light (2.99×10^8 ms^{-1}), E_g = Bandgap energy, and λ = Wavelength (Absorption peak value). 1eV = 1.6×10^{-19} Joules (Conversion factor).

By rearranging equation 3 or 4, a model relative to a straight-line graph equation is obtained and is given by;

$$\alpha_{direct}\,(hv) = A\,(hv - Eg)^{\frac{1}{2}} \tag{5}$$

$$\alpha_{indirect}\,(hv) = B\,(hv - Eg)^2 \tag{6}$$

Thus, the bandgap of a perovskite semiconductor is estimated from the intercept of the extrapolated linear fit for the plotted experimental data of $\alpha^{(1/2)}$ versus incident photon energy (hν) near the absorption edge.

However, crystalline perovskite thin films might have some disordered and non-stoichiometric species that result in a poor or low crystallinity structure which causes passivation of the surface. This leads to a localised UV-absorption tail known as the Urbach tail, [49]. Consequently, the Urbach energy equation can be applied to determine the perovskite structural disorder and is given by.

$$\propto = \propto \star exp^{(E/E_u)} \tag{7}$$

$\propto$ = Absorption coefficient, $\propto_*$ = constant, E = the photon energy, E_u = Urbach energy, which denotes the energy of the band tail. The Urbach energy is weakly dependent on temperature and is interpreted as the width of the band tail in a normal band gap that is associated with a disorder or low perovskite crystallinity. Thus, by taking the natural logarithm of Eq. (7), a straight-line graph equation is obtained and is given by.

$$ln \propto = ln \propto_* + (\tfrac{hv}{Eu}) \tag{8}$$

Hence, the Urbach energy (Band Tail) is determined from the slope of a straight-line graph by plotting In $\propto$ against incident photon energy (hν), A graphical illustration of the bandgap and Urbach tail is presented in Fig. 10 [50].

4.1. Perovskite thin-film X-ray characterisation

X-ray analyses can provide information about the crystalline structure and properties of perovskite. The information provided by this characterisation technique can be employed to study the crystalline structure, the crystallisation process of perovskite, as well as the possible presence of deleterious unreacted species (for example PbI_2) [51]. During the transition of $CH_3NH_3PbI_3$ from α cubic phase to β tetragonal phase at 54 °C–60 °C, the cubic (100) peak splits into two signals (002) and (110) [52], the same phenomenon happens for other planes in the same family. The relative intensity between these two peaks provides information about the quality of perovskite thin film. (110) orientation seems to be associated with higher crystallinity and more stability than (002) [53]· irrespective of the technique used to grow the perovskite. (002) is usually formed in non-equilibrium conditions

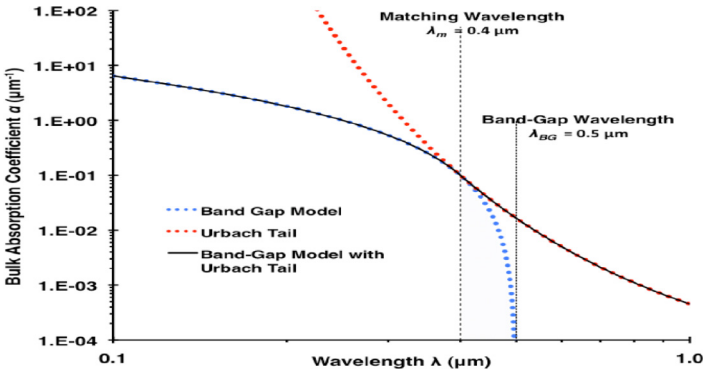

Fig. 10. Graphical illustration of Urbach-tail and bandgap determination of a semiconductor from UV–Vis absorbance [50].

such as electrospray deposition without annealing [54], conversion of PbI_2 into perovskite using a low-temperature MAI bath [51], or fast-flux rates during evaporation of perovskite [55], Scattering intensity associated with (002) can be converted into (110) when the perovskite films are treated at high temperatures within the limit of transition to α cubic phase, or by decreasing the flux rate of evaporation. Perovskites with predominantly (110) X-ray scattering exhibit higher light absorption, less rough morphology, and higher conductivity [54]. When solar cells are fabricated with the active perovskite layer that predominantly shows (110) scattering, higher J_{SC} and PCE are observed [51].

Some properties, in particular, microstrain, present inside the perovskite lattice might cause changes to the degree of crystal orientation which could also have a direct consequence on the performance of solar cells [51]. Microstrain is the consequence of small variations in the lattice spacing, due to imperfections or defects within the perovskite thin-film, such as vacancies, dislocations, twinning and grain boundaries [56]. Microstrain can be generated during the nucleation and growth of perovskite thin films [57] and after their annealing due to differences in the expansion coefficient of perovskite and the underlying substrate [58], the composition of the perovskite also influences microstrain, through the dimension of the A-cation [59]. As microstrain is decreased the PCE of perovskite solar cells increases [59]. A possible explanation for this behaviour was given by *Zhu et al.* who discovered a correlation between regions with small microstrains, long carrier lifetime and low defect density, suggesting that the microstrain can induce the formation of disordered states acting as recombination centres [60,61]. Another hypothesis states that the microstrains induce valence band bending, therefore modifying the carrier dynamics [62]. As a consequence, the energy gap of perovskite varies, it decreases for compressive microstrains and increases for tensile microstrains [62].

4.2. Current–voltage curve and power conversion efficiency

One of the fundamental properties of perovskite thin-film PVs is the conversion of the incident light radiation to electric current, the efficiency of this conversion can be determined from the current–voltage curve (i.e., I–V curve) [63]. An I–V curve is a graphical representation that explains the relationship between the voltage applied across an electrical device and the current that flows through it. This curve is obtained by load switching that involves the use of different resistor loads connected across a source of power, a voltmeter, and an ammeter to measure the voltage and current output respectively [63]. Some of the parameters that could be determined from the I–V curves include open-circuit voltage (V_{oc}), short circuit current (I_{sc}), series resistance (R_s), shunt resistance (R_{sh}), fill factor (FF), maximum power point (P_{mp}) and solar cell power conversion efficiency (PCE or η). At zero resistance, maximum current is produced while for a load of infinite resistance, the maximum voltage is generated. FF is a solar cell performance indicator which is ideally as close to 1 as possible. It is related to the squareness of the IV curve and can be obtained from the ratio of the area of two rectangles on an IV plot, one defined by the origin, I_{sc} and V_{oc} (that represents the most ideal I–V curve) and the other by the origin and the maximum power point on the current–voltage graph [63]. Additionally, the magnitude of FF depends on the module design and technology. i.e., generally, crystalline silicon PV modules have higher FF than amorphous silicon PVs while Perovskite PVs have higher FF than Organic solar cells. However, the effects of mismatch soiling of the active PV

layers with the ETL/HTL might cause series losses and shunt losses which result in an impairment in the FF [63]. This causes a reduction in the power output by reducing either the I_{mp}, V_{mp}, or both I_{mp} and V_{mp}. Thus, resulting in I–V hysteresis. Generally, hysteresis refers to the fluctuation in the current–voltage response curve thereby leading to inconsistency in the photovoltaics parameters. This phenomenon significantly affects device performance and also hinders the accurate determination of the PCE. Ferroelectric polarisation, capacitive effect, Ion migration and trapping of electronic carriers at the perovskite interface were reported as the major course of I–V hysteresis [64].

5. Perovskite solar cell fabrication

High-quality perovskite thin films are crucial for the development of high-performing perovskite photovoltaic devices. In this context, that means the film will have uniform morphology and coverage of the substrate, with high areal density (the presence of pinholes will be minimised) and consist of large grains. For clarification, a grain is a unit of material in which the crystal structure is the same throughout and is bounded on all sides by grain boundaries with other grains, interfaces, or a surface. Minimising pinholes is important because in devices pinholes will present a region where the light will not be absorbed and can lead to shunt paths through which there will be a leakage current. Uniform morphology and coverage are required because the surface needs to be consistent in its coverage to ensure the conformal deposition of succeeding device layers. This can be obtained by having widespread uniform and dense nucleation of the perovskite crystals during crystallisation. These challenges are approached through solvent engineering of the precursor solution, and optimisation of the deposition and subsequent annealing processes in terms of time, temperature, and atmosphere. Grains of a size comparable to the thickness of the perovskite film will reduce the number of grain boundaries. Grain boundaries are typically more disordered than the grain bulk because the grain boundaries possess more defects such as vacancies or inclusions which act as trap states to charge carriers. A higher density of trap states (particularly Shockley-Read-Hall defects) results in recombination of charge carriers and will hence reduce the device performance. Grain boundaries also facilitate the migration of ions or environmentally introduced species such as oxygen [65]. Furthermore, films with smaller grains have shown lower fracture resistance, with the grain boundaries providing favourable paths for crack propagation [66]. Grains that are oriented preferentially relative to the substrate can also help to improve charge carrier extraction. A film with more ordered grains and higher crystallinity is typically desirable, and this is an aspect routinely measured using X-ray diffraction techniques, transmission electron microscopy (TEM), and to a lesser extent, scanning electron microscopy (SEM). Large grains oriented preferentially with regards to the substrate (or charge transfer layer) tend to generally lead to better performing PSCs, although there are examples of high-performing PSCs with small grains [67].

Charge carrier lifetime and diffusion length are another two metrics typically used to characterise thin films for photovoltaics. These reflect the average time it will take and the distance a photogenerated carrier will move before it can be expected to undergo recombination with another carrier — either radiatively, emitting a photon, or non-radiatively, where the energy is lost as heat in the form of phonons propagating through the lattice as the carrier falls to a lower energy trap state (trap-mediated recombination) or by energy transfer to another charge carrier in the CB or VB (Auger recombination). Long carrier lifetimes and long diffusion lengths are typically interpreted as being indicative of low trap-state density and low rates of non-radiative recombination. These values can be measured and explored using measurements of photoluminescence quantum yield (PLQY), time-resolved photoluminescence spectroscopy (TRPL), and surface photovoltage (SPV) measurements [68]. The reactivity of metal halide perovskites is particularly important during the processing, deposition, and formation of films. Compositional changes or doping effects can occur due to reaction with oxygen, H_2O, and additives to the precursor solution, or even simply due to the volatility of the species in the film, with MA halides being particularly volatile [69]. This can lead to detrimental changes to optoelectronic properties due to the formation of traps. Redox chemistry is also important in the decomposition of perovskite films, with Zhao et al. observing the spontaneous reaction of perovskites with Al, Cr, Ag, and Yb, reducing the Pb^{2+} cations to Pb^0. This occurred even in the absence of typical triggering factors of moisture, light or oxygen [70]. The degradation of hybrid perovskite films will be elaborated upon in later sections. For $MAPbI_3$, the thermodynamic stability of the pure 3D perovskite phase lies within a very narrow range of compositions of its binary halide precursor components. Local decomposition can easily occur due to these reactions, typically leading to secondary phases such as PbI_2. PbI_2 is often observed passivating the perovskite at grain boundaries and interfaces, reducing the number of trap states. It is itself photoactive and may contribute to charge carrier generation. However too much of this phase presents an obstacle to charge carrier transport and

stability, and if present it needs to be optimised to maintain high film quality [71]. Other secondary phases at best will act as dead zones in the film, but at worst will act as nucleation points for the further degradation of the film into non-perovskite phases. The formation of such phases needs to be minimised to maintain homogeneous film properties and retain high charge carrier lifetimes, mobility, and extraction.

5.1. Solution processing of Perovskite solar cell

One-step deposition via spin coating of a precursor solution is one of the simplest and most accessible techniques for preparing perovskite thin films for solar cells. The solution is prepared by dissolving precursor materials such as MAI or PbI_2 in a polar solvent such as dimethylformamide (DMF) or dimethyl sulfoxide (DMSO), or mixtures thereof. The solution is dropped onto a spinning substrate immediately before or during rotation at thousands of revolutions per minute, which centrifugally spreads the solution over the wetted surface. Initially, removal of an excess solution is dominated by the angular force as the substrate spins, while in the latter stages of spin casting evaporation dominates. The surface chemistry of the substrate must be compatible with the solution such that it wets the surface easily to form a continuous film. Depending on when the spinning stops, evaporation may continue in subsequent drying or annealing. As the solvent is removed, the precursors increase in concentration until they become supersaturated in the remaining solution and begin to precipitate out of the solution, nucleating and beginning the conversion to perovskite as they react. Some perovskite systems, such as $MAPbI_3$ in γ-butyrolactone (GBL) and $MAPbBr_3$ in DMF show inverse solubility, where solubility decreases with an increase in temperature, allowing for rapid crystal growth at elevated temperature [72]. The nucleation process can be described using the Lamer model as shown in Fig. 11a of homogeneous nucleation [73], where solvated precursor molecules in solution increase in concentration with evaporation time until they hit the super-saturation limit [73]. At this point, homogeneous nucleation occurs as the concentration of precursors hits a critical level for the perovskite formation reaction to occur. The conversion of precursor solvates to the nucleating perovskite phase reduces the concentration of precursor in solution, reducing it below the super-saturation concentration, and reducing further nucleation. At this point growth of existing nuclei dominates.

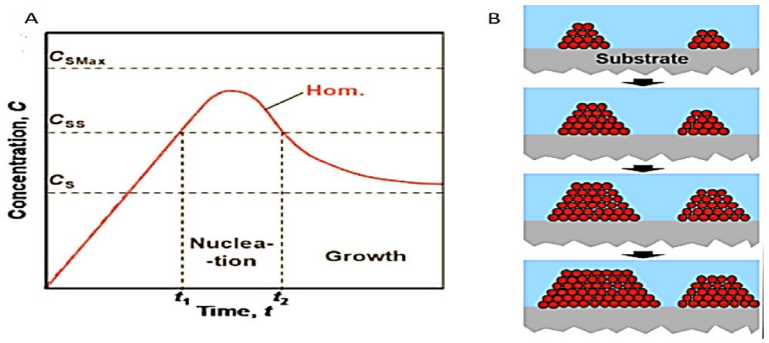

Fig. 11. Graph of Lamer model of crystal growth assuming homogeneous nucleation [73]. b) Volmer–Weber mode Island Growth of crystallites [74].

In practice, a combination of homogeneous and heterogeneous nucleation occurs, with heterogeneous nucleation dominating at low saturation, and homogeneous nucleation dominating at high saturation and above the super saturation limit. For controlled nucleation and growth of precursors from solution, usually heterogeneous nucleation of the perovskite nuclei on the substrate material is required, as opposed to homogeneous nucleation within a solution, as the latter can result in poor film coverage. The substrate reduces the energy barrier for nucleation by reducing the interfacial energy of the liquid and crystal interface [75]. A useful model for describing crystal growth is the Volmer–Weber mode (see Fig. 11b), where the nucleating phase forms as separate islands on the substrate, and therefore a high density of nuclei arising from the evaporating solution is required to ensure a dense, uniform thin film forms [74]. However, this model was designed to describe deposition from a gaseous phase and not from a solvent, so cannot capture the full picture of perovskite crystal growth. However, Volmer–Weber

does not require an epitaxial relationship with the substrate and is hence useful for describing perovskite film growth, where crystallisation may begin at the solvent-air interface for example. To obtain a high-quality film, an optimum between nucleation density and crystal growth must be reached. If the nucleation density is too high, a very fine-grained structure will form with many grain boundaries, requiring subsequent heat treatment to grow grains and reduce grain boundaries, defects, and interfacial strain. If nucleation density is too low, large grains with gaps between them will develop. These gaps will not absorb light and can provide shunting paths where the current will be lost in a device, or even shorting paths if selective charge transport layers come into contact through these holes in the photoactive film layer. To control the film formation and prevent these issues, many approaches have been developed, from solvent engineering and thermal engineering (controlling the heating regime) to surface and interfacial engineering (manipulating the chemistry of surfaces to control film formation) using post-deposition treatments or use of additives in the precursor solution.

To address the issue of large, poorly connected grains, solvent engineering methods have been developed which mainly aim to stimulate a high rate of nucleation over a short period as possible, reducing the time available for dendritic structures to grow (which led to a discontinuous film). One way this can be achieved is by the application of nonpolar anti-solvents during spin casting. Anti-solvents rapidly raise the saturation of the solute by simultaneously reducing the solubility of the precursors in the solution and increasing the evaporation rate of the solvent (as solvent molecules are less strongly conjugated with solute molecules they will more readily evaporate). Examples include toluene, chlorobenzene, and ethyl acetate [76], The rapid nucleation that results from the application of an anti-solvent leads to a desirable, compact, dense grain structure. Another approach to achieving this is through vacuum drying after spin casting. This has been used to quickly remove solvent from the film [77]. Gas quenching to accelerate solvent evaporation and rapidly raise supersaturation of the solution has also been used [78]. The solvent itself can be changed to achieve the desired rate of supersaturation; for example, the spin-casting from a mixture of methylamine (MA) and acetonitrile (ACN) delivers films with uniform, the compact microstructure of large, smooth grains. The perovskite nucleates very rapidly during spin-coating as the solvents rapidly evaporate. Furthermore, the deposited films have carrier lifetimes 20 times greater than those from films prepared using DMF, suggesting the use of this method also reduces defects [77]. Solvent annealing methods are yet another technique developed to improve thin-film microstructure and morphology. Annealing in a solvent vapour atmosphere results in larger grain size and improved crystallinity [79]. It is thought that this may occur due to the dissolution of material at grain boundaries and surfaces in a solvent phase, allowing the reordering of crystals, and grain boundary migration. Huang et al. used DMF solvent vapour during the annealing of $MAPbI_3$ to obtain 1 μm grains with dramatically improved electrical properties in comparison to films that were simply thermally annealed. The champion device had a PCE of 15.6% [79]. It is also common to use a mixture of solvents to attain the desired nucleation and growth of the perovskite phase, most typically DMF and DMSO. The high solubility of precursors in DMF is combined with the longer film drying times offered by solvents like DMSO. As a result, many researchers have sought to understand the influence of solvent choice on perovskite film formation [80].

5.2. Perovskite thin-film degradation

Unpackaged perovskite solar cells degrade within a few hundred hours of exposure to air with a relative humidity greater than 50% [81]. Moisture induces a combination of reversible and irreversible changes in the film, depending on the extent of exposure. Many metal halide perovskites are relatively stable when left in the dark, but they will rapidly degrade when in the presence of oxygen and light, through the light-accelerated process of photo-oxidation. Therefore, oxidation resistance is also desirable. Rand et al. performed a comprehensive study of the chemistry of perovskite optoelectronic devices [70]. They found redox chemistry plays an underlying role in determining the degradation processes in perovskite devices with Ag/Al/Yb/Cr metal contacts. In-situ XRD revealed the spontaneous reduction of Pb^{2+} to Pb^0 in the presence of Al^0, converting $MAPbI_3 \rightarrow MA_4PbI_6{\cdot}2H_2O \rightarrow MAI$. In-situ SEM shows that H_2O facilitates ion diffusion, enabling the continued reaction of the Al and perovskite layers. While not necessary for the redox reaction to occur, it facilitates the diffusion of unreacted Lead Iodide to the Al^0 electrode. What their study emphasised was that degradation investigations need to focus on the whole device and not just the individual layers, as critical chemical reactions can stem from intrinsic interfacial interactions between layers. Moisture's role as a decomposition reagent in perovskite films is only secondary to the more dominant device degradation pathways at metal contact interfaces, where moisture facilitates the reduction of the perovskite. H_2O

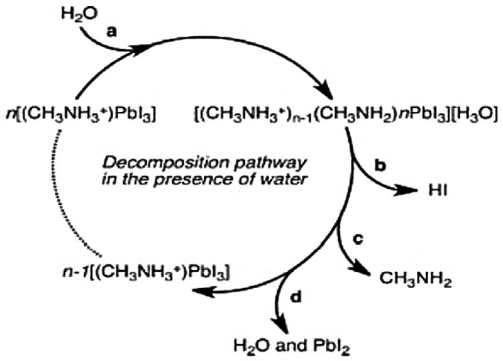

Fig. 12. Potential moisture-initiated decomposition pathway [83].

molecules in the perovskite form strong H-bonds with organic cations, weakening the bond between the cation and PbI_6-octahedral cage. This enables more rapid deprotonation (removal of Hydrogen) of the organic cation, which leaves the perovskite more susceptible to the deleterious effects of exposure to electrical fields or heat [82]. Water reacts with iodide (I^-) to create hydroiodic acid. This reaction leaves PbI_2 after decomposition. Frost et al. propose the decomposition pathway (Fig. 12) [83]. H_2O is required to initiate the reaction, producing soluble HI, volatile, gaseous methylamine (CH_3NH_2), and finally H_2O and PbI_2 [83].

Tuning the perovskite structure by X-site and A-site substitution such that the 3D perovskite structure is retained when the film is exposed to moisture is one strategy to improve moisture resilience. The lattice parameters and bond environment remain more similar to the cubic or tetragonal perovskite upon extended exposure to moisture, suggesting doped perovskites are more resilient to decomposition due to reaction with H_2O. Haque et al. have thoroughly investigated the decomposition reaction of lead halide perovskites, finding that diffusion of O_2 into bulk $MAPbI_3$ films occurs immediately upon exposure to air, and is complete within an hour [65]. Oxygen adsorbs at iodide vacancies on the surface and diffuses through iodide vacancies in the bulk [65]. Iodine vacancies (V_I) have an intrinsically high concentration and are rapidly generated upon photoexcitation. Once oxygen is adsorbed at vacancy sites, the O_2 in V_I sites act as traps for photo-excited electrons in the conduction band. The O_2 becomes reduced to a superoxide species; O_2^-. The negatively charged species reacts with highly positively charged A-site protonated cations in an acid–base reaction that creates H_2O, lead iodide and deprotonated A-site gas such as methylamine. It would follow that less acidic A-site cations such as formamidinium or caesium will be more stable to photo-oxidation. It is critical to control the density of iodide vacancies in perovskite films to suppress the adsorption of O_2 at these sites, and diffusion through the bulk. This can be achieved by similar structural tuning methods as described before, as well as surface passivation techniques [84].

6. Conclusion

Perovskite photovoltaics have rapidly risen to become one of the research frontiers with the most potential to compete with thin-film microcrystalline silicon PVs. It is paramount to understand the working principles, materials, architecture, and fabrication processes of perovskite thin films to make highly efficient solar cells. As such, we have explained the fundamental paths to which effective perovskite photovoltaics can be made. The major challenge with perovskite PVs is their stability and we hope this piece of work will provide the basis that results in a stability breakthrough.

Declaration of competing interest

The authors declare that they have no known competing financial interests or personal relationships that could have appeared to influence the work reported in this paper.

Data availability

No data was used for the research described in the article.

Acknowledgements

This work was financially supported by the Petroleum Technology Development Fund (PTDF-Nigeria) for S.B. via Ph.D studentship with grant code PTDF/ED/OSS/PHD/SAB/1677/19 at the University of sheffield, and the UK Engineering and Physical Sciences Research Council (EPSRC) via a Ph.D. studentship for A.U., F.B. also at the University of Sheffield from the Centre for Doctoral Training in New and Sustainable Photovoltaics, with grant code EP/L01551X/2.

References

[1] Hurley S. Opportunities for solar energy. 2021, Explaining Science Solar Energy: WorldPress.com. Available at: https://explainingscience.org/2021/10/18/opportunities-for-solar-energy/ (Accessed: 14 February 2022).
[2] Blum AS, Jähnert M. The birth of quantum mechanics from the spirit of radiation theory. Stud Hist Philos Sci 2022;91:125–47.
[3] Li Z, Kim TH, Han SY, Yun Y-J, Jeong S, Jo B, et al. Wide-bandgap perovskite/gallium arsenide tandem solar cells. Adv Energy Mater 2020a;10(6):1903085.
[4] NREL. Best research-cell efficiency chart. 2022, U.S Department of Energy: NREL. Available at: https://www.nrel.gov/pv/cell-efficiency.html. (Accessed: 20 February 2022).
[5] Kojima A, Teshima K, Shirai Y, Miyasaka T. Organometal halide perovskites as visible-light sensitizers for photovoltaic cells. J Am Chem Soc 2009;131(17):6050–1.
[6] Hussain I, Tran HP, Jaksik J, Moore J, Islam N, Uddin MJ. Functional materials, device architecture, and flexibility of perovskite solar cell. Emergent Mater 2018;1(3):133–54.
[7] Gopal Krishna B, Rathore GS, Shukla N, Tiwari S. 18 - Perovskite solar cells: A review of architecture, processing methods, and future prospects. In: Khan I, Khan A, Khan MMA, Khan S, Verpoort F, Umar A, editors. Hybrid Perovskite Composite Materials. Woodhead Publishing; 2021, p. 375–412.
[8] Kumaresan P, Vegiraju S, Ezhumalai Y, Yau SL, Kim C, Lee W-H, et al. Fused-thiophene based materials for organic photovoltaics and dye-sensitized solar cells. Polymers 2014;6(10).
[9] You J, Meng L, Hong Z, Li G, Yang Y. Inverted planar structure of perovskite solar cells. In: Organic-inorganic halide perovskite photovoltaics. Springer; 2016, p. 307–24.
[10] Miyata A, Mitioglu A, Plochocka P, Portugall O, Wang JT-W, Stranks SD, et al. Direct measurement of the exciton binding energy and effective masses for charge carriers in organic–inorganic tri-halide perovskites. Nat Phys 2015;11(7):582–7.
[11] Shubbak MH. Advances in solar photovoltaics: Technology review and patent trends. Renew Sustain Energy Rev 2019;115:109383.
[12] Richter A, Hermle M, Glunz SW. Reassessment of the limiting efficiency for crystalline silicon solar cells. IEEE J Photovolt 2013;3(4):1184–91.
[13] Richter A, Glunz SW, Werner F, Schmidt J, Cuevas A. Improved quantitative description of auger recombination in crystalline silicon. Phys Rev B 2012;86(16):165202.
[14] Li Z, Kim TH, Han SY, Yun YJ, Jeong S, Jo B, et al. Wide-bandgap perovskite/gallium arsenide tandem solar cells. Adv Energy Mater 2020b;10(6):1903085.
[15] Yuan J, Zhang Y, Zhou L, Zhang G, Yip H-L, Lau T-K, et al. Single-junction organic solar cell with over 15% efficiency using fused-ring acceptor with electron-deficient core. Joule 2019;3(4):1140–51.
[16] Tang CW. Two-layer organic photovoltaic cell. Appl Phys Lett 1986;48(2):183–5.
[17] Brabec CJ, Gowrisanker S, Halls JJM, Laird D, Jia S, Williams SP. Polymer–fullerene bulk-heterojunction solar cells. Adv Mater 2010;22(34):3839–56.
[18] Optoelectronics. Organic photovoltaics. 2022, Cavendish Laboratory, Cambridge: The University of Cambridge Available at: https://www.oe.phy.cam.ac.uk/research/photovoltaics/ophotovoltaics. (Accessed: 26 February 2022).
[19] Resch-Genger U, Grabolle M, Cavaliere-Jaricot S, Nitschke R, Nann T. Quantum dots versus organic dyes as fluorescent labels. Nature Methods 2008;5(9):763.
[20] Qiao Q. Organic solar cells: materials, devices, interfaces, and modeling. CRC Press; 2017.
[21] Rand BP, Richter H. Organic solar cells: fundamentals, devices, and upscaling. CRC Press; 2014.
[22] Jamalullail N, Mohamad IS, Norizan MN, Baharum NA, Mahmed N. Short review: Natural pigments photosensitizer for dye-sensitized solar cell (DSSC). In: 2017 IEEE 15th Student Conference on Research and Development. p. 344–9.
[23] Wu Y, Zhu W. Organic sensitizers from D–π–A to D–A–π–A: effect of the internal electron-withdrawing units on molecular absorption, energy levels and photovoltaic performances. Chem Soc Rev 2013;42(5):2039–58.
[24] Fakharuddin A, Jose R, Brown TM, Fabregat-Santiago F, Bisquert J. A perspective on the production of dye-sensitized solar modules. Energy Environ Sci 2014;7(12):3952–81.
[25] Pramono SH, Maulana E, Prayogo AF, Djatmika R. Characterization of dye-sensitized solar cell (DSSC) based on chlorophyll dye. Int J Appl Eng Res 2015;10(1):193–205.
[26] Arkenstone T. Perovskite (sharp crystals). 2021, United State of America (USA): American Gen Trade association (AGTA). Available at: https://www.irocks.com/minerals/specimen/43725. (Accessed: 21 March 2021).
[27] Hazen RM. Perovskites. Sci Am 1988;258(6):74–81.
[28] Bartel CJ, Sutton C, Goldsmith BR, Ouyang R, Musgrave CB, Ghiringhelli LM, et al. New tolerance factor to predict the stability of perovskite oxides and halides. Sci Adv 2019;5(2):eaav0693.

[29] Hwang T, Lee B, Kim J, Lee S, Gil B, Yun AJ, et al. From nanostructural evolution to dynamic interplay of constituents: perspectives for perovskite solar cells. Adv Mater 2018;30(42):1704208.
[30] Green MA, Ho-Baillie A, Snaith HJ. The emergence of perovskite solar cells. Nat Photonics 2014;8(7):506–14.
[31] Whitmire KH. Bismuth: Inorganic chemistry. In: Encyclopedia of inorganic and bioinorganic chemistry. 2011, p. 1–32.
[32] Savill KJ, Ulatowski AM, Herz LM. Optoelectronic properties of tin–lead halide perovskites. ACS Energy Lett 2021;6(7):2413–26.
[33] Philippe B, Saliba M, Correa-Baena J-P, Cappel UB, Turren-Cruz S-H, Grätzel M, et al. Chemical distribution of multiple cation (Rb+, Cs+, MA+, and FA+) perovskite materials by photoelectron spectroscopy. Chem Mater 2017;29(8):3589–96.
[34] Meng X, Bai Y, Xiao S, Zhang T, Hu C, Yang Y, et al. Designing new fullerene derivatives as electron transporting materials for efficient perovskite solar cells with improved moisture resistance. Nano Energy 2016;30:341–6.
[35] Han GS, Yoo JS, Yu F, Duff ML, Kang BK, Lee J-K. Highly stable perovskite solar cells in humid and hot environment. J Mater Chem A 2017;5(28):14733–40.
[36] Sani F, Shafie S, Lim HN, Musa AO. Advancement on lead-free organic–inorganic halide perovskite solar cells: a review. Materials 2018;11(6):1008.
[37] Chen P, Bai Y, Lyu M, Yun JH, Hao M, Wang L. Progress and perspective in low-dimensional metal halide perovskites for optoelectronic applications. Solar Rrl 2018;2(3):1700186.
[38] Assadi MK, Bakhoda S, Saidur R, Hanaei H. Recent progress in perovskite solar cells. Renew Sustain Energy Rev 2018;81:2812–22.
[39] Song Z, Watthage SC, Phillips AB, Tompkins BL, Ellingson RJ, Heben MJ. Impact of processing temperature and composition on the formation of methylammonium lead iodide perovskites. Chem Mater 2015;27(13):4612–9.
[40] Ran C, Xu J, Gao W, Huang C, Dou S. Defects in metal triiodide perovskite materials towards high-performance solar cells: origin, impact, characterization, and engineering. Chem Soc Rev 2018;47(12):4581–610.
[41] Maksym V, Kovalenko LP, Bodnarchuk MI. Properties and potential optoelectronic applications of lead halide perovskite nanocrystals. Science 2017;358:745–50.
[42] Buin A, Pietsch P, Xu J, Voznyy O, Ip AH, Comin R, et al. Materials processing routes to trap-free halide perovskites. Nano Lett 2014;14(11):6281–6.
[43] Lee J-W, Kim S-G, Bae S-H, Lee D-K, Lin O, Yang Y, et al. The interplay between trap density and hysteresis in planar heterojunction perovskite solar cells. Nano Lett 2017;17(7):4270–6.
[44] Braly IL, deQuilettes DW, Pazos-Outón LM, Burke S, Ziffer ME, Ginger DS, et al. Hybrid perovskite films approaching the radiative limit with over 90% photoluminescence quantum efficiency. Nat Photonics 2018;12(6):355–61.
[45] Eames C, Frost JM, Barnes PRF, O'Regan BC, Walsh A, Islam MS. Ionic transport in hybrid lead iodide perovskite solar cells. Nature Commun 2015;6(1):7497.
[46] Yue L, Yan B, Attridge M, Wang Z. Light absorption in perovskite solar cell: Fundamentals and plasmonic enhancement of infrared band absorption. Sol Energy 2016;124:143–52.
[47] Stegeman GI, Miller A. Physics of all-optical switching devices. In: Midwinter JE, editor. Photonics in switching. San Diego: Academic Press; 1993, p. 81–145 [chapter 5].
[48] Soga T. Fundamentals of solar cell. In: Soga T, editor. Nanostructured materials for solar energy conversion. Amsterdam: Elsevier; 2006, p. 3–43 [chapter 1].
[49] Sharma N, Prabakar K, Ilango S, Dash S, Tyagi AK. Optical band-gap and associated Urbach energy tails in defected AlN thin films grown by ion beam sputter deposition: Effect of assisted ion energy. 2017, p. 342–6.
[50] Moosmüller H, Chakrabarty RK, Ehlers KM, Arnott WP. Absorption Ångström coefficient, brown carbon, and aerosols: basic concepts, bulk matter, and spherical particles. Atmos Chem Phys 2011;11(3):1217–25.
[51] Docampo P, Hanusch FC, Giesbrecht N, Angloher P, Ivanova A, Bein T. Influence of the orientation of methylammonium lead iodide perovskite crystals on solar cell performance. Apl Mater 2014;2(8):081508.
[52] Kavadiya S, Strzalka J, Niedzwiedzki DM, Biswas P. Crystal reorientation in methylammonium lead iodide perovskite thin film with thermal annealing. J Mater Chem A 2019;7(20):12790–9.
[53] Borchert J, Boht H, Fränzel W, Csuk R, Scheer R, Pistor P. Structural investigation of co-evaporated methyl ammonium lead halide perovskite films during growth and thermal decomposition using different PbX 2 (X=I, Cl) precursors. J Mater Chem A 2015;3(39):19842–9.
[54] Im J-H, Lee C-R, Lee J-W, Park S-W, Park N-G. 6.5% Efficient perovskite quantum-dot-sensitized solar cell. Nanoscale 2011;3(10):4088–93.
[55] Kim H-S, Lee C-R, Im J-H, Lee K-B, Moehl T, Marchioro A, et al. Lead iodide perovskite sensitized all-solid-state submicron thin film mesoscopic solar cell with efficiency exceeding 9%. Sci Rep 2012;2(1):1–7.
[56] Wang JT-W, Wang Z, Pathak S, Zhang W, deQuilettes DW, Wisnivesky-Rocca-Rivarola F, et al. Efficient perovskite solar cells by metal ion doping. Energy Environ Sci 2016;9(9):2892–901.
[57] McMeekin DP, Wang Z, Rehman W, Pulvirenti F, Patel JB, Noel NK, et al. Crystallization kinetics and morphology control of formamidinium–cesium mixed-cation lead mixed-halide perovskite via tunability of the colloidal precursor solution. Adv Mater 2017;29(29):1607039.
[58] Zhao J, Deng Y, Wei H, Zheng X, Yu Z, Shao Y, et al. Strained hybrid perovskite thin films and their impact on the intrinsic stability of perovskite solar cells. Sci Adv 2017;3(11):eaao5616.
[59] Nishimura K, Hirotani D, Kamarudin MA, Shen Q, Toyoda T, Iikubo S, et al. Relationship between lattice strain and efficiency for Sn-perovskite solar cells. ACS Appl Mater Interfaces 2019;11(34):31105–10.
[60] Zhu X, Yang D, Yang R, Yang B, Yang Z, Ren X, et al. Superior stability for perovskite solar cells with 20% efficiency using vacuum co-evaporation. Nanoscale 2017;9(34):12316–23.

[61] Zhu C, Niu X, Fu Y, Li N, Hu C, Chen Y, et al. Strain engineering in perovskite solar cells and its impacts on carrier dynamics. Nature Commun 2019;10(1):1–11.
[62] Grote C, Berger RF. Strain tuning of tin–halide and lead–halide perovskites: a first-principles atomic and electronic structure study. J Phys Chem C 2015;119(40):22832–7.
[63] Sarikh S, Raoufi M, Bennouna A, Benlarabi A, Ikken B. Implementation of a plug and play I-V curve tracer dedicated to characterization and diagnosis of PV modules under real operating conditions. Energy Convers Manage 2020;209:112613.
[64] Elumalai NK, Uddin A. Hysteresis in organic–inorganic hybrid perovskite solar cells. Sol Energy Mater Sol Cells 2016;157:476–509.
[65] Aristidou N, Eames C, Sanchez-Molina I, Bu X, Kosco J, Islam MS, et al. Fast oxygen diffusion and iodide defects mediate oxygen-induced degradation of perovskite solar cells. Nature Commun 2017;8(1):1–10.
[66] Hamzavy BT, Grieco WJ, Fields BJ, Libby CS, Hobbs WB, Lavrova O, et al. Study of PV Module Degradation Rate Prediction Through Correlation of Field-Aged and Accelerated-Aged Module Degradation Data. IEEE; 2017, p. 2618–21.
[67] Stolterfoht M, Wolff CM, Amir Y, Paulke A, Perdigón-Toro L, Caprioglio P, et al. Approaching the fill factor Shockley–Queisser limit in stable, dopant-free triple cation perovskite solar cells. Energy Environ Sci 2017;10(6):1530–9.
[68] Danekamp B, Droseros N, Palazon F, Sessolo M, Banerji N, Bolink HJ. Efficient photo-and electroluminescence by trap states passivation in vacuum-deposited hybrid perovskite thin films. ACS Appl Mater Interfaces 2018;10(42):36187–93.
[69] Dar MI, Hinderhofer A, Jacopin G, Belova V, Arora N, Zakeeruddin SM, et al. Function follows form: correlation between the growth and local emission of perovskite structures and the performance of solar cells. Adv Funct Mater 2017;27(26):1701433.
[70] Zhao L, Kerner RA, Xiao Z, Lin YL, Lee KM, Schwartz J, et al. Redox chemistry dominates the degradation and decomposition of metal halide perovskite optoelectronic devices. ACS Energy Lett 2016;1(3):595–602.
[71] Meier T, Gujar TP, Schönleber A, Olthof S, Meerholz K, van Smaalen S, et al. Impact of excess PbI 2 on the structure and the temperature dependent optical properties of methylammonium lead iodide perovskites. J Mater Chem C 2018;6(28):7512–9.
[72] Saidaminov MI, Abdelhady AL, Murali B, Alarousu E, Burlakov VM, Peng W, et al. High-quality bulk hybrid perovskite single crystals within minutes by inverse temperature crystallization. Nature Commun 2015;6(1):1–6.
[73] LaMer VK, Dinegar RH. Theory, production and mechanism of formation of monodispersed hydrosols. J Am Chem Soc 1950;72(11):4847–54.
[74] Venables JA, Spiller GDT. Nucleation and growth of thin films. Surf Mobil Solid Mater 1983;34:1–404.
[75] Zhou Y, Game OS, Pang S, Padture NP. Microstructures of organometal trihalide perovskites for solar cells: their evolution from solutions and characterization. J Phys Chem Lett 2015;6(23):4827–39.
[76] Kong M, Hu H, Egbo K, Dong B, Wan L, Wang S. Anti-solvent assisted treatment for improved morphology and efficiency of lead acetate derived perovskite solar cells. Chin Chem Lett 2019;30(6):1325–8.
[77] Ding B, Gao L, Liang L, Chu Q, Song X, Li Y, et al. Facile and scalable fabrication of highly efficient lead iodide perovskite thin-film solar cells in air using gas pump method. ACS Appl Mater Interfaces 2016;8(31):20067–73.
[78] Conings B, Babayigit A, Klug M, Bai S, Gauquelin N, Sakai N, et al. Getting Rid of Anti-Solvents: Gas Quenching for High Performance Perovskite Solar Cells. IEEE; 2018, p. 1724–9.
[79] Nie W, Tsai H, Asadpour R, Blancon J-C, Neukirch AJ, Gupta G, et al. High-efficiency solution-processed perovskite solar cells with millimeter-scale grains. Science 2015;347(6221):522–5.
[80] Jung M, Ji S-G, Kim G, Seok SI. Perovskite precursor solution chemistry: from fundamentals to photovoltaic applications. Chem Soc Rev 2019;48(7):2011–38.
[81] Yang J, Siempelkamp BD, Liu D, Kelly TL. Investigation of CH3NH3PbI3 degradation rates and mechanisms in controlled humidity environments using in situ techniques. ACS Nano 2015;9(2):1955–63.
[82] Divitini G, Cacovich S, Matteocci F, Cinà L, Di Carlo A, Ducati C. In situ observation of heat-induced degradation of perovskite solar cells. Nat Energy 2016;1(2):1–6.
[83] Frost JM, Butler KT, Brivio F, Hendon CH, van Schilfgaarde M, Walsh A. Atomistic origins of high-performance in hybrid halide perovskite solar cells. Nano Lett 2014;14(5):2584–90.
[84] Saidaminov MI, Kim J, Jain A, Quintero-Bermudez R, Tan H, Long G, et al. Suppression of atomic vacancies via incorporation of isovalent small ions to increase the stability of halide perovskite solar cells in ambient air. Nat Energy 2018;3(8):648–54.